

## Modeling and Simulation of a Quantum Thermal Noise on the Qubit

François Chapeau-Blondeau

*Laboratoire Angevin de Recherche en Ingénierie des Systèmes (LARIS)*  
*Université d'Angers, 62 Avenue Notre Dame du Lac*  
*49000 Angers, France*  
*\*chapeau@univ-angers.fr*

Received 30 June 2022

Accepted 10 August 2022

Published 24 September 2022

Communicated by Laszlo B. Kish

Quantum noise or decoherence is a major factor impacting the performance of quantum technologies. On the qubit, an important quantum noise, often relevant in practice, is the thermal noise or generalized amplitude damping noise, describing the interaction with a thermal bath at an arbitrary temperature. A qubit thermal noise however cannot be modeled nor directly simulated with a few elementary Pauli operators, but instead requires specific operators. Our main goal here is to construct a circuit model for simulating the thermal noise from standard elementary qubit operators. Starting from a common quantum-operation model based on Kraus operators and an associated qubit-environment model, we derive a proper Stinespring dilated representation for the thermal noise. This dilated unitary model is then decomposed in terms of simple elementary qubit operators, and converted into a circuit based on elementary quantum gates. We arrive at our targeted simulator circuit for the thermal noise, coming with built-in easy control on the noise parameters. The noise simulator is then physically implemented and tested on an IBM-Q quantum processor. The simulator represents a useful addition to existing libraries of quantum circuits for quantum processors, and it offers a new tool for investigating quantum signal and information processing having to cope with thermal noise.

*Keywords:* Quantum noise; quantum signal; noise modeling; noise simulation; quantum processor; decoherence.

### 1. Introduction

At the quantum level, quantum noise or decoherence represents the alteration of quantum states or signals caused by their interaction with an uncontrolled environment [1–3]. Quantum noise is a major factor impacting the performance of quantum technologies and quantum information processing [4–6]. It is therefore essential to take quantum noise into account when designing, testing and developing quantum methodologies and devices. In this respect, both theoretical modeling and

controlled physical simulation are important elements for coping with quantum noise in quantum technologies. For the fundamental system of quantum technologies constituted by the qubit, there exist common noises, such as the bit-flip noise, the phase-flip noise, and the depolarizing noise, whose action can be conveniently modeled with a few elementary Pauli operators [1, 3]. With such a simple and generic constitution, these noises are relatively easy to handle and can be rather directly simulated from elementary gates available in circuit libraries of current quantum processors. Another very important qubit noise is the quantum thermal noise or generalized amplitude damping noise [1, 7, 8], which describes the interaction of the qubit with a thermal bath at an arbitrary temperature, and which is therefore frequently relevant in practice. However, by contrast, this noise does not possess a simple model based on the standard Pauli operators, but instead requires specific operators. These specific operators are not found in the gate libraries of standard quantum processors. As a consequence, this thermal noise model is not associated with a known direct circuit implementation from elementary gates. In this study, we target to arrive at such a simulator circuit for the qubit thermal noise, implementable with elementary gates available in libraries of standard quantum processors, and enabling controlled physical simulation.

Our starting point is a common quantum-operation model for the thermal noise based on four Kraus operators and an associated qubit-environment model. From these elements, we derive a proper Stinespring dilated model for the thermal noise. The dilated unitary representation is then decomposed and expressed by means of simple elementary qubit operators. This decomposition is then converted into a simulator circuit for the thermal noise, constituted by elementary quantum gates, with also built-in easy control on the parameters of the thermal noise. This quantum circuit is then physically implemented and tested on an IBM-Q quantum processor accessible online, to validate that it behaves according to the theoretical specifications of the thermal noise model. In this way, the results deliver the targeted quantum circuit for controlled simulation of the qubit thermal noise on quantum processors, offering a new tool for design and test in quantum signal and information processing.

## 2. Modeling of the Qubit Thermal Noise

### 2.1. *Kraus operator-sum representation*

A quantum thermal noise or generalized amplitude damping noise acting on a qubit with 2-dimensional Hilbert space  $\mathcal{H}_2$  is commonly modeled [1, 8] by means of the four Kraus operators with matrix representation relative to the computational basis

$$\Lambda_1 = \sqrt{p} \begin{bmatrix} 1 & 0 \\ 0 & \sqrt{1-\gamma} \end{bmatrix}, \quad (1)$$

$$\Lambda_2 = \sqrt{p} \begin{bmatrix} 0 & \sqrt{\gamma} \\ 0 & 0 \end{bmatrix}, \quad (2)$$

$$\Lambda_3 = \sqrt{1-p} \begin{bmatrix} \sqrt{1-\gamma} & 0 \\ 0 & 1 \end{bmatrix}, \quad (3)$$

$$\Lambda_4 = \sqrt{1-p} \begin{bmatrix} 0 & 0 \\ \sqrt{\gamma} & 0 \end{bmatrix}. \quad (4)$$

On a qubit with density operator  $\rho \in \mathcal{L}(\mathcal{H}_2)$ , the thermal noise realizes the quantum operation

$$\rho \mapsto \rho' = \mathcal{N}(\rho) = \sum_{k=1}^4 \Lambda_k \rho \Lambda_k^\dagger. \quad (5)$$

Such a noise provides a model [1, 8], useful to quantum technologies, to describe the interaction of a qubit with an uncontrolled environment representing a thermal bath at temperature  $T$ . The parameter  $\gamma \in [0, 1]$  is a damping or coupling factor which often can be expressed as a function of the interaction time  $t$  of the qubit with the bath as  $\gamma = 1 - e^{-t/\tau_1}$ , where  $\tau_1$  is a time constant for the interaction (such as the spin-lattice relaxation time  $\tau_1$  in magnetic resonance). At long interaction times  $t \gg \tau_1$ , then  $\gamma \rightarrow 1$  and the qubit relaxes to the equilibrium or thermalized mixed state  $\rho_\infty = p|0\rangle\langle 0| + (1-p)|1\rangle\langle 1|$ . At equilibrium, the qubit has probabilities  $p$  of being measured in the ground state  $|0\rangle$  and  $1-p$  of being measured in the excited state  $|1\rangle$ . With the energies  $E_0$  and  $E_1 > E_0$ , respectively, for the states  $|0\rangle$  and  $|1\rangle$ , the equilibrium probabilities are governed by the Boltzmann distribution, giving

$$p = \frac{\exp[-E_0/(k_B T)]}{\exp[-E_0/(k_B T)] + \exp[-E_1/(k_B T)]} = \frac{1}{1 + \exp[-(E_1 - E_0)/(k_B T)]}, \quad (6)$$

and providing the connection between the temperature  $T$  and the probability  $p$ . As  $T \rightarrow 0$  the probability  $p \rightarrow 1$  for the ground state  $|0\rangle$ , while at  $T \rightarrow \infty$  the ground state  $|0\rangle$  and excited state  $|1\rangle$  become equiprobable with  $p = 1/2$ . From Eq. (6), when the temperature  $T$  monotonically increases above 0 up to  $\infty$ , the probability  $p$  monotonically decreases from 1 to 1/2.

When the input density operator has matrix representation  $\rho = [\rho_{00}, \rho_{01}; \rho_{01}^*, 1 - \rho_{00}]$  in the computational basis, the transformed (output) noisy density operator delivered by Eq. (5) follows as

$$\mathcal{N}(\rho) = \begin{bmatrix} (1-\gamma)\rho_{00} + \gamma p & \sqrt{1-\gamma}\rho_{01} \\ \sqrt{1-\gamma}\rho_{01}^* & 1 - (1-\gamma)\rho_{00} - \gamma p \end{bmatrix}. \quad (7)$$

## 2.2. Stinespring dilated unitary representation

An alternative model for the qubit thermal noise is by means of a Stinespring dilated unitary representation [1, 2, 9, 10]. This approach involves the introduction of a

model for the environment and its interaction with the qubit, in order to deduce an evolution of the qubit state equivalent to Eq. (5). Such a model is especially necessary when one wants to design a quantum circuit so as to physically simulate, in a controlled way, the effect of the thermal noise on the qubit. In turn, such physical noise simulators are useful to test quantum signal or information processing methodologies and algorithms under controlled noise conditions. In addition, novel quantum phenomena recently investigated and involving a non-unitary evolution of a qubit as in Eq. (5), require for their complete determination an explicit reference to a model for the underlying environment producing the non-unitary evolution [11, 12].

For a principal quantum system  $Q$  (here our qubit prepared in state  $\rho$ ) with Hilbert space  $\mathcal{H}_Q$  and experiencing a non-unitary evolution  $\rho \mapsto \mathcal{N}(\rho)$ , a Stinespring dilated unitary representation introduces an environment  $E$  with Hilbert space  $\mathcal{H}_E$ . The environment  $E$  is prepared in a pure quantum state  $|e_0\rangle \in \mathcal{H}_E$ . The system-environment compound  $QE$  forms a closed quantum system, starting in the separable bipartite state  $\rho \otimes |e_0\rangle\langle e_0|$ , and undergoing a joint unitary evolution by the unitary operator  $\mathbf{U}_{QE}$ . The evolved bipartite state is then reduced by partial tracing over the environment  $E$ , so as to obtain the reduced density operator

$$\rho' = \text{tr}_E [\mathbf{U}_{QE} (\rho \otimes |e_0\rangle\langle e_0|) \mathbf{U}_{QE}^\dagger] \quad (8)$$

resulting for the principal system  $Q$ . By the Stinespring dilation theorem [13, 1], any operator-sum representation as in Eq. (5) defining a valid non-unitary evolution  $\rho \mapsto \rho' = \mathcal{N}(\rho)$ , can be obtained by such a tensoring to a larger (dilated) system that is unitarily evolved and then reduced by partial tracing as in Eq. (8).

For a given quantum operation  $\mathcal{N}(\cdot)$  defined by a set of Kraus operators  $\{\Lambda_k\}_{k=1}^K$  as in Eq. (5) with  $K = 4$ , the task is then to select an environment model with its initial state  $|e_0\rangle$  and a joint unitary evolution  $\mathbf{U}_{QE}$ , so as to satisfy  $\rho' = \mathcal{N}(\rho)$  in Eq. (8). This can be achieved in a infinite number of ways. There however exists a canonical procedure as follows. For any pure state  $|Q\rangle \in \mathcal{H}_Q$  of the principal system  $Q$ , and initial state  $|e_0\rangle \in \mathcal{H}_E$  of the environment  $E$ , the joint unitary evolution  $\mathbf{U}_{QE}$  is defined by

$$\mathbf{U}_{QE}|Q\rangle \otimes |e_0\rangle = \sum_{k=1}^K \Lambda_k |Q\rangle \otimes |e_k\rangle = |\psi'_{QE}\rangle, \quad (9)$$

where  $\{|e_k\rangle\}_{k=1}^K$  is an orthonormal basis of the  $K$ -dimensional space  $\mathcal{H}_E$  chosen for the environment  $E$ . The density operator associated with the bipartite state  $|\psi'_{QE}\rangle$  of Eq. (9) is

$$\rho'_{QE} = |\psi'_{QE}\rangle\langle\psi'_{QE}| = \sum_{k=1}^K \sum_{k'=1}^K \Lambda_k |Q\rangle\langle Q| \Lambda_{k'}^\dagger \otimes |e_k\rangle\langle e_{k'}|, \quad (10)$$

which upon partial tracing over the environment  $E$  provides the reduced density operator for the principal quantum system  $Q$  as

$$\rho' = \text{tr}_E(\rho'_{QE}) = \sum_{k=1}^K \Lambda_k |Q\rangle\langle Q| \Lambda_k^\dagger, \quad (11)$$

matching the targeted quantum operation defined by the Kraus operators  $\{\Lambda_k\}_{k=1}^K$ . An initial mixed state  $\rho$  of the principal system  $Q$  transforms in the same way, as a convex sum of pure states like  $|Q\rangle\langle Q|$ , by linearity of Eq. (11).

To obtain an environment model simulating the quantum thermal noise according to this procedure, the  $K = 4$  Kraus operators  $\Lambda_k$  of Eqs. (1)–(4) imply a 4-dimensional environment  $E$ , achievable with a pair of qubits referred to the orthonormal basis  $\{|e_k\rangle\}_{k=1}^4 = \{|00\rangle, |01\rangle, |10\rangle, |11\rangle\}$  of  $\mathcal{H}_E \equiv \mathcal{H}_2^{\otimes 2}$ . Then, for an arbitrary pure state  $|Q\rangle = \alpha_0|0\rangle + \alpha_1|1\rangle \in \mathcal{H}_2$  of the input qubit, Eq. (9) leads to

$$\mathbf{U}_{QE}|Q\rangle \otimes |e_0\rangle = \Lambda_1|Q\rangle \otimes |00\rangle + \Lambda_2|Q\rangle \otimes |01\rangle + \Lambda_3|Q\rangle \otimes |10\rangle + \Lambda_4|Q\rangle \otimes |11\rangle \quad (12)$$

$$= \sqrt{p}[\alpha_0|000\rangle + \alpha_1\sqrt{\gamma}|001\rangle + \alpha_1\sqrt{1-\gamma}|100\rangle] \\ + \sqrt{1-p}\left[\alpha_0\sqrt{1-\gamma}|010\rangle + \alpha_1|110\rangle + \alpha_0\sqrt{\gamma}|111\rangle\right], \quad (13)$$

that must be satisfied by selecting  $\mathbf{U}_{QE}$  and  $|e_0\rangle$ .

For a useful noise simulator which we target here, it is important to devise an efficient control over the thermal noise parameters  $(p, \gamma)$ . One potential solution could be to seek to control the noise parameters  $(p, \gamma)$  by means of the initial state  $|e_0\rangle \in \mathcal{H}_2^{\otimes 2}$  of the two-qubit environment model, associated with a fixed  $(p, \gamma)$ -independent unitary  $\mathbf{U}_{QE}$  in Eqs. (12) and (13). One could try for instance the separable state  $|e_0\rangle = (\sqrt{p}|0\rangle + \sqrt{1-p}|1\rangle) \otimes (\sqrt{\gamma}|0\rangle + \sqrt{1-\gamma}|1\rangle)$ , or else a more involved entangled state. Then, usually  $|e_0\rangle$  will vary in the 4-dimensional space  $\mathcal{H}_2^{\otimes 2}$  when  $(p, \gamma)$  cover  $[0, 1]^2$ . With  $|Q\rangle$  covering  $\mathcal{H}_2$ , the joint state  $|Q\rangle \otimes |e_0\rangle$  will in general vary in the 8-dimensional space  $\mathcal{H}_2^{\otimes 3}$ . However, Eq. (13) shows that the three-qubit transformed state  $\mathbf{U}_{QE}|Q\rangle \otimes |e_0\rangle$  assumes no component in the subspace spanned by  $\{|011\rangle, |101\rangle\}$  and therefore remains in a 6-dimensional subspace of  $\mathcal{H}_2^{\otimes 3}$ . Since the 8-dimensional space  $\mathcal{H}_2^{\otimes 3}$  cannot be unitarily mapped onto the 6-dimensional subspace defined by Eq. (13), no control of  $(p, \gamma)$  can be generally achieved via the initial state  $|e_0\rangle$  associated with a fixed  $(p, \gamma)$ -independent unitary  $\mathbf{U}_{QE}$  satisfying Eqs. (12) and (13).

### 3. A Simulator Circuit

Instead, to guide a useful selection of the constituents  $(|e_0\rangle, \mathbf{U}_{QE})$  of the environment model, especially affording efficient control of the noise parameters  $(p, \gamma)$ , we will make use of a model [8, 14] inspired from a bosonic channel for a single optical mode coupled to another (dissipating) optical mode at a beamsplitter with transmittivity  $1 - \gamma$  and reflectivity  $\gamma$ . When one of the input arms (mode) on the beamsplitter

contains no photon, then in the incident arm (mode), a photon is transmitted unaltered with probability  $1 - \gamma$ , while it is reflected into the other output arm (mode) with the complementary probability  $\gamma$  [8]. This model is known as the thermal attenuator [8, 14], and it exhibits some formal equivalence with the qubit thermal noise we are interested in. In the thermal attenuator, the environment is represented by a 2-dimensional quantum system prepared in the mixed state  $\rho_\infty = p|0\rangle\langle 0| + (1 - p)|1\rangle\langle 1|$  determined by the equilibrium or thermalized state of the thermal bath. The input qubit and the 2-dimensional environment interact through the unitary operator

$$U_{th} = \begin{bmatrix} 1 & 0 & 0 & 0 \\ 0 & \sqrt{1-\gamma} & \sqrt{\gamma} & 0 \\ 0 & -\sqrt{\gamma} & \sqrt{1-\gamma} & 0 \\ 0 & 0 & 0 & 1 \end{bmatrix}, \quad (14)$$

evolving the bipartite state  $\rho \otimes \rho_\infty \mapsto U_{th}(\rho \otimes \rho_\infty)U_{th}^\dagger$ . Then it is easily verified that partial tracing of this transformed state over the environment produces the state  $\mathcal{N}(\rho)$  of Eq. (7). However, strictly speaking, with this model based on Eq. (14) given in [8], we are not dealing for the qubit thermal noise  $\mathcal{N}(\cdot)$  with a proper Stinespring dilated representation as in Eq. (8). The reason is that in this noise model based on Eq. (14) the environment starts in a mixed qubit state  $\rho_\infty$ , while a proper Stinespring dilated representation [1, 2, 9, 10] requires an environment starting in a pure state as  $|e_0\rangle$  in Eq. (8). It is possible to obtain a proper Stinespring dilated representation as in Eq. (8), and at the same time, for our purpose of constructing a simulator circuit for the thermal noise, obtain an easy control on the noise parameter  $p$ . This is accomplished by introducing a purification of the initial state  $\rho_\infty$  of the environment. This can be realized by resorting to an additional auxiliary qubit, which is entangled to the environment qubit by a preparation in the pure two-qubit state  $\sqrt{p}|00\rangle + \sqrt{1-p}|11\rangle$ ; then partial tracing on the auxiliary qubit places the environment qubit in the targeted mixed state  $\rho_\infty = p|0\rangle\langle 0| + (1 - p)|1\rangle\langle 1|$ . Moreover, in practice this operation is easily accomplished by a Cnot gate fed by a target qubit in state  $|0\rangle$  and a control qubit in state  $|p\rangle = \sqrt{p}|0\rangle + \sqrt{1-p}|1\rangle$ . The two qubits at the Cnot output terminate in the joint entangled pure state  $\sqrt{p}|00\rangle + \sqrt{1-p}|11\rangle$ . When the target qubit is then discarded (non-measured), the resulting uncertainty is described by partial tracing of the joint state over the target qubit, and the control qubit gets placed in the mixed state  $\rho_\infty = p|0\rangle\langle 0| + (1 - p)|1\rangle\langle 1|$  as expected [1, 2]. A quantum circuit achieving this

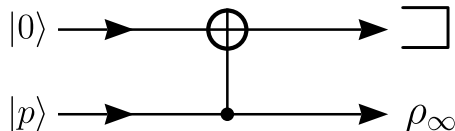


Fig. 1. Control of the parameter  $p$  of the thermal noise: The Cnot gate is fed by a target qubit in state  $|0\rangle$  and a control qubit in state  $|p\rangle = \sqrt{p}|0\rangle + \sqrt{1-p}|1\rangle$ . On the two-qubit output state  $\sqrt{p}|00\rangle + \sqrt{1-p}|11\rangle$ , when the target qubit is discarded, the control qubit is described by the mixed state  $\rho_\infty = p|0\rangle\langle 0| + (1 - p)|1\rangle\langle 1|$ .

process is depicted in Fig. 1, that when input with a control qubit in state  $|p\rangle = \sqrt{p}|0\rangle + \sqrt{1-p}|1\rangle$  will provide the targeted control on the parameter  $p$  of the thermal noise.

The process illustrated in Fig. 1 restores a proper Stinespring dilated representation for the qubit thermal noise  $\mathcal{N}(\cdot)$ , with a two-qubit environment model prepared in the pure state  $\sqrt{p}|00\rangle + \sqrt{1-p}|11\rangle = |e_0\rangle$  along with a joint dilated unitary evolution acting trivially on the auxiliary qubit initialized in state  $|0\rangle$  in Fig. 1, and giving in Eq. (8) the three-qubit unitary  $\mathbf{U}_{QE} = \mathbf{U}_{\text{th}} \otimes \mathbf{I}_2$ . Also, an advantage in proceeding in this way for constructing a simulator model for the qubit thermal noise, is that we obtain a convenient separated control of the noise parameters  $(p, \gamma)$ : the probability  $p$  is controlled via an auxiliary qubit in the initial state  $|p\rangle = \sqrt{p}|0\rangle + \sqrt{1-p}|1\rangle$  of Fig. 1, while the coupling factor  $\gamma$  is controlled via the unitary  $\mathbf{U}_{\text{th}}$  of Eq. (14).

It is also useful to seek a simple implementation of the two-qubit unitary  $\mathbf{U}_{\text{th}}$  of Eq. (14). Based on their universality property for the synthesis of quantum circuits [1, 15], we know that the two-qubit Cnot gate complemented by one-qubit gates can offer an implementation for  $\mathbf{U}_{\text{th}}$  as well as for any unitary operator. Such a synthesis can be carried out by applying the generic procedure described in [1, 15], that we apply and report here for the first time for a simulator of the qubit thermal noise. The procedure would start by decomposing the unitary operator into two-level unitary matrices, which is always feasible in principle [1] (two-level unitary matrices are unitary matrices that act non-trivially only on two or fewer vector components). Here, our unitary matrix of interest  $\mathbf{U}_{\text{th}}$  in Eq. (14) is already a two-level unitary matrix, acting non-trivially only on the two vector components along  $|01\rangle$  and  $|10\rangle$ . The two-level part of the matrix  $\mathbf{U}_{\text{th}}$  is extracted as

$$\tilde{\mathbf{U}} = \begin{bmatrix} \sqrt{1-\gamma} & \sqrt{\gamma} \\ -\sqrt{\gamma} & \sqrt{1-\gamma} \end{bmatrix}. \quad (15)$$

The two-level unitary  $\mathbf{U}_{\text{th}}$  of Eq. (14), when it acts on the compound  $QE$  of the principal qubit  $Q$  and environment qubit  $E$ , implements a transformation that can be decomposed into the sequence of three elementary unitary transformations defined in Fig. 2 by their action on the computational basis of  $\mathcal{H}_2^{\otimes 2}$ .

$QE$	$T_1$	$QE$	$\tilde{\mathbf{U}}c$	$QE$	$T_1^{-1} \equiv T_1$	$QE$
$ 00\rangle$	$\mapsto$	$ 00\rangle$	$\mapsto$	$ 00\rangle$	$\mapsto$	$ 00\rangle$
$ 01\rangle$	$\mapsto$	$ 01\rangle$	$\mapsto$	$(\sqrt{1-\gamma} 0\rangle - \sqrt{\gamma} 1\rangle) 1\rangle$	$\mapsto$	$\sqrt{1-\gamma} 01\rangle - \sqrt{\gamma} 10\rangle$
$ 10\rangle$	$\mapsto$	$ 11\rangle$	$\mapsto$	$(\sqrt{\gamma} 0\rangle + \sqrt{1-\gamma} 1\rangle) 1\rangle$	$\mapsto$	$\sqrt{\gamma} 01\rangle + \sqrt{1-\gamma} 10\rangle$
$ 11\rangle$	$\mapsto$	$ 10\rangle$	$\mapsto$	$ 10\rangle$	$\mapsto$	$ 11\rangle$

Fig. 2. The sequence of three elementary unitary transformations  $T_1$ , then the controlled  $\tilde{\mathbf{U}}c$  from Eq. (15), and finally  $T_1^{-1} \equiv T_1$ , acting on the qubit pair  $QE$ , to realize the unitary transformation  $\mathbf{U}_{\text{th}}$  of Eq. (14).

The first transformation  $T_1$  in Fig. 2 rearranges the vector components for the qubit pair  $QE$  so that the two-level transformation of Eq. (14) gets applied only to one (the qubit  $Q$ ) of the two quits. This transformation  $T_1$  amounts to a controlled-not on the qubit  $E$  controlled by the qubit  $Q$ , and will therefore receive a simple circuit implementation with a Cnot gate. The second transformation  $\tilde{U}_c$  in Fig. 2 is the one-qubit unitary  $\tilde{U}$  of Eq. (15), acting only on qubit  $Q$  yet under the control of qubit  $E$ . We will therefore have to obtain a controlled version of the one-qubit gate  $\tilde{U}$  of Eq. (15). The third transformation in Fig. 2 restores the initial arrangement of the vector components for the qubit pair  $QE$ , via the inverse transformation  $T_1^{-1} \equiv T_1$  coinciding with  $T_1$ . After the sequence of Fig. 2, the state of the qubit pair  $QE$  has experienced the targeted unitary transformation  $U_{th}$  in Eq. (14). The sequence of Fig. 2 can be given a simple circuit implementation depicted in Fig. 3.

We now want to work out a simple circuit implementation for the controlled gate  $\tilde{U}_c$  used in Fig. 3, that is, a circuit where a control qubit at  $|1\rangle$  applies the gate  $\tilde{U}$  to the target qubit, while a control qubit at  $|0\rangle$  leaves the target qubit unaffected. For this purpose, we follow the generic procedure of [1, 15] to construct a controlled version of an arbitrary one-qubit gate. The unitary transformation  $\tilde{U}$  of Eq. (15) is a rotation in the space  $\mathcal{H}_2$  by the angle  $\xi \in [-\pi/2, 0]$  defined by  $\cos(\xi) = \sqrt{1-\gamma}$  and  $\sin(\xi) = -\sqrt{\gamma}$ , that is  $\xi = -\arcsin(\sqrt{\gamma})$ . It is convenient to introduce the standard one-qubit gate  $R_y(\xi)$  defined by the rotation matrix

$$R_y(\xi) = \exp\left(-i\frac{\xi}{2}Y\right) = \begin{bmatrix} \cos(\xi/2) & -\sin(\xi/2) \\ \sin(\xi/2) & \cos(\xi/2) \end{bmatrix}, \quad (16)$$

so that  $\tilde{U} = R_y(2\xi)$ . More importantly for our purpose, we also have  $\tilde{U} = R_y(\xi)X R_y(-\xi)X$ , with the standard inversion or “not” Pauli matrix  $X = [0, 1; 1, 0]$ . This decomposition for  $\tilde{U}$  can be verified by directly performing the matrix products; it also results from [15, Lemma 4.3] or [1, Corollary 4.2] on p. 176. In addition we have  $R_y(\xi)R_y(-\xi) = I_2$ . It results that if we apply the control on  $X$  with a standard Cnot gate, we obtain the controlled gate  $\tilde{U}_c$  that is targeted. The circuit implementation of this procedure is depicted in Fig. 4.

Now we can assemble the three quantum circuits of Figs. 1, 3 and 4 so as to obtain the simulator circuit for the quantum thermal noise on the qubit with arbitrary parameters  $(p, \gamma)$ , as represented in Fig. 5.

The circuit of Fig. 5 realizes a Stinespring dilated unitary representation according to the principles of Sec. 2.2, to simulate the qubit thermal noise  $\mathcal{N}(\cdot)$ .

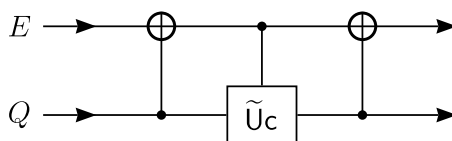


Fig. 3. Quantum circuit implementation realizing on the qubit pair  $QE$  the unitary transformation  $U_{th}$  of Eq. (14) via the decomposition of Fig. 2, and using a controlled version  $\tilde{U}_c$  of the gate  $\tilde{U}$  from Eq. (15).

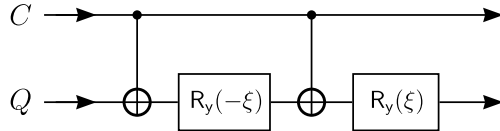


Fig. 4. Quantum circuit implementation of the controlled gate  $\tilde{U}c$  used in Fig. 3, featuring two one-qubit standard  $R_y$  rotation gates from Eq. (16) and two Cnot gates, and applying the transformation  $\tilde{U}$  to the target qubit  $Q$  under the control of the qubit  $C$ .

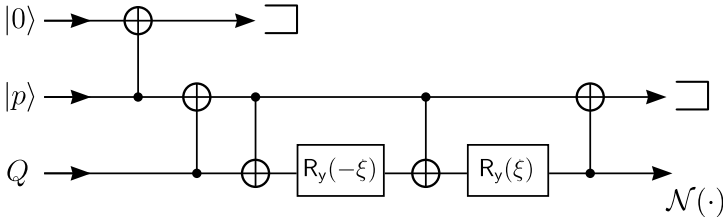


Fig. 5. Quantum circuit simulating the quantum thermal noise  $N(\cdot)$  defined by the quantum operation of Eqs. (1)–(5) on the principal qubit  $Q$ . The input auxiliary qubit in state  $|p\rangle = \sqrt{p}|0\rangle + \sqrt{1-p}|1\rangle \in \mathcal{H}_2$  sets the parameter  $p$  of the thermal noise. The two one-qubit rotation gates  $R_y(\cdot)$  with the angle  $\xi = -\arcsin(\sqrt{\gamma})$  set the parameter  $\gamma$  of the thermal noise.

defined by the quantum operation of Eqs. (1)–(5). The four Kraus operators in Eqs. (1)–(4) for the qubit thermal noise determine a 4-dimensional environment implemented by two auxiliary qubits in Fig. 5, in addition to the principal qubit  $Q$  experiencing the thermal noise, for a total of three qubits used by the noise simulator. The two auxiliary environment qubits are initialized in the pure separable state  $|p\rangle \otimes |0\rangle$ , with the qubit prepared in state  $|p\rangle = \sqrt{p}|0\rangle + \sqrt{1-p}|1\rangle$  enabling one to adjust the parameter  $p$  of the thermal noise. The quantum circuit of Fig. 5 to simulate the qubit thermal noise  $N(\cdot)$  relies only on elementary quantum gates: 5 two-qubit Cnot gates and 2 one-qubit rotation gates  $R_y(\cdot)$ . The angle  $\xi = -\arcsin(\sqrt{\gamma})$  for the rotation gates enables one to adjust the parameter  $\gamma$  of the thermal noise. The two environment qubits in the circuit of Fig. 5 are discarded (non-measured), and the circuit output marked  $N(\cdot)$  delivers the noisy qubit affected by the thermal noise with controlled parameters  $(p, \gamma)$ .

In the special case with  $p = 1$ , the qubit thermal noise reduces to the amplitude damping noise [1], defined by only two nonzero Kraus operators  $\Lambda_1$  and  $\Lambda_2$  in place of the four operators of Eqs. (1)–(4), and it describes the interaction of the qubit with a thermal bath at a zero temperature  $T = 0$ . In this special case, the control state  $|p\rangle$  in Fig. 5 reduces to the state  $|0\rangle$ , and our circuit of Fig. 5 is equivalent to the quantum circuit for modeling amplitude damping given in Fig. 8.13 of [1]. The more general circuit of Fig. 5 is a contribution to extend the noise modeling to an arbitrary temperature  $T$ .

#### 4. Physical Implementation and Test

The simulator circuit of Fig. 5 for the qubit thermal noise has been physically implemented and tested on an IBM quantum processor publicly accessible online on the web [16–22]. The quantum circuit is described via the graphical composer of the front-end interface of the IBM processor. The circuit description invokes a library of built-in elementary quantum gates available on the processor (which motivates the necessity of decomposing into elementary gates the quantum operation of the qubit thermal noise, as undertaken in Sec. 3). Among standard elementary gates in the IBM quantum library are the two-qubit Cnot gate, and the one-qubit rotation gate  $R_y(\xi)$  at an arbitrary angle  $\xi$ . The circuit layout for the thermal noise simulator of Fig. 5 is displayed in Fig. 6, while the code issued to describe the circuit is given in Fig. 7.

The input qubit state  $|p\rangle = \sqrt{p}|0\rangle + \sqrt{1-p}|1\rangle$  used in the simulator of Fig. 5 to set the probability  $p$  of the thermal noise, is realized in the circuit of Fig. 6 by an additional rotation gate  $R_y(\xi_p)$  with angle  $\xi_p = 2\arccos(\sqrt{p})$ , fed with the input state  $|0\rangle$  and outputting  $|p\rangle$  (acting on the qubit  $q_1$  in Fig. 6).

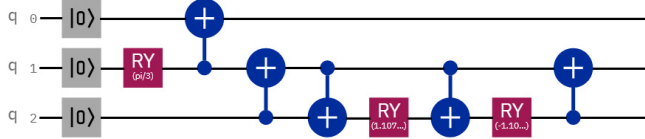


Fig. 6. Circuit layout from the front-end graphical composer interface of the IBM quantum processor, implementing the simulator of Fig. 5 for the qubit thermal noise.

```

OPENQASM 2.0;
include "qelib1.inc";

qreg q[3];
creg c[3];

reset q[0];
reset q[1];
reset q[2];
ry(pi/3) q[1];
cx q[1],q[0];
cx q[2],q[1];
cx q[1],q[2];
ry(1.107148717794090) q[2];
cx q[1],q[2];
ry(-1.107148717794090) q[2];
cx q[2],q[1];
  
```

Fig. 7. Code generated by the IBM graphical composer interface to describe the quantum circuit layout of Fig. 6.

With the noise simulator running on the quantum processor, for various states  $|Q\rangle$  of the input qubit  $Q$  (the qubit  $q_2$  in Fig. 6), quantum measurements on the output noisy state  $\mathcal{N}(|Q\rangle\langle Q|)$  were performed, for different configurations of the parameters  $(p, \gamma)$  of the thermal noise. In particular, the probability  $\Pr\{|Q\rangle\} = \langle Q|\mathcal{N}(|Q\rangle\langle Q|)|Q\rangle$  of measuring the output state  $\mathcal{N}(|Q\rangle\langle Q|)$  in the input state  $|Q\rangle$  was evaluated, which here equivalently represents the squared fidelity [1] of the output state  $\mathcal{N}(|Q\rangle\langle Q|)$  with the input state  $|Q\rangle$ . The experimental results are presented in Figs. 8–10.

In the tests of Figs. 8–10, for a given state  $|Q\rangle$  of the input qubit  $Q$ , the probabilities of the measurement outcomes on the output noisy state  $\mathcal{N}(|Q\rangle\langle Q|)$  are theoretically predicted from the model of Eq. (7). For comparison, the same measurement probabilities are also theoretically evaluated, from the circuit layout of Fig. 6, by means of the preprocessing simulator associated with the IBM quantum processor. The results of Figs. 8–10 always show an excellent match between the theoretical probabilities resulting from Eq. (7) and those computed by the preprocessing simulator. This validates that the simulator circuit designed in Fig. 5 indeed behaves according to the specifications of the quantum thermal noise model of Eqs. (1)–(5). Finally for comparison, the measurement probabilities have been experimentally evaluated from the physical implementation of the noise simulator of Figs. 5 and 6. The implementation has been executed on the “ibmq\_bogota” quantum processor from [16]. For each data point in Figs. 8–10, the run of the quantum circuit with the final output measurement was repeated  $10^4$  times, and the corresponding probability value evaluated as a relative frequency. A batch of  $10^4$  runs typically took around 10 s on the quantum processor. The IBM quantum processors,

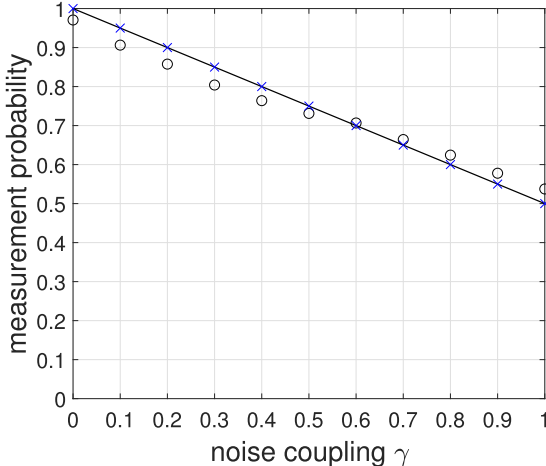


Fig. 8. For a noise probability  $p = 1/2$  (high temperature range) and an input qubit  $Q$  in state  $|0\rangle$ , the probability  $\Pr\{|0\rangle\} = \langle 0|\mathcal{N}(|0\rangle\langle 0|)|0\rangle$  of measuring the output noisy qubit in the state  $|0\rangle$ , as a function of the coupling parameter  $\gamma$  of the thermal noise. The solid line is the theoretical model  $\Pr\{|0\rangle\} = \gamma p + 1 - \gamma = 1 - \gamma/2$  from Eq. (7). The crosses ( $\times$ ) show the theoretical value computed by the preprocessing simulator from the circuit layout. The open circles ( $\circ$ ) show the experimental evaluation.

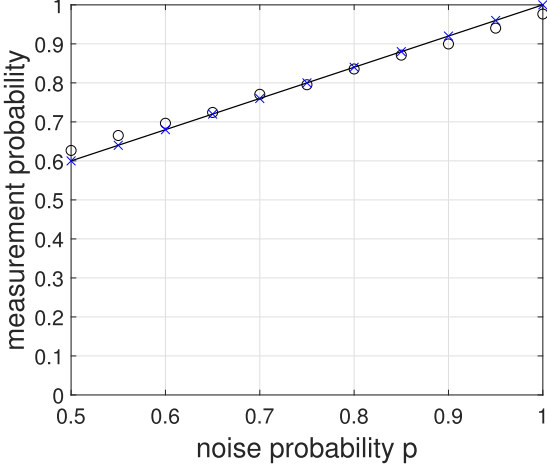


Fig. 9. For a noise coupling  $\gamma = 0.8$  and an input qubit  $Q$  in state  $|0\rangle$ , the probability  $\text{Pr}\{|0\rangle\} = \langle 0|\mathcal{N}(|0\rangle\langle 0|)|0\rangle$  of measuring the output noisy qubit in the state  $|0\rangle$ , as a function of the probability  $p$  of the thermal noise. The solid line is the theoretical model  $\text{Pr}\{|0\rangle\} = \gamma p + 1 - \gamma = 0.8p + 0.2$  from Eq. (7). The crosses ( $\times$ ) show the theoretical value computed by the preprocessing simulator from the circuit layout. The open circles ( $\circ$ ) show the experimental evaluation.

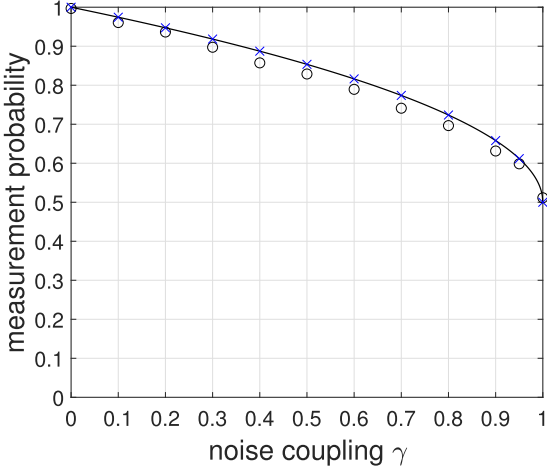


Fig. 10. For a noise probability  $p = 3/4$  and an input qubit  $Q$  in state  $|+\rangle$ , the probability  $\text{Pr}\{|+\rangle\} = \langle +|\mathcal{N}(|+\rangle\langle +|)|+\rangle$  of measuring the output noisy qubit in the state  $|+\rangle$ , as a function of the coupling parameter  $\gamma$  of the thermal noise. The solid line is the theoretical model  $\text{Pr}\{|+\rangle\} = (1 + \sqrt{1 - \gamma})/2$  from Eq. (7). The crosses ( $\times$ ) show the theoretical value computed by the preprocessing simulator from the circuit layout. The open circles ( $\circ$ ) show the experimental evaluation.

based on superconducting qubits, have inherent imperfections. As a result, some discrepancy is observed between the experimental and theoretical probabilities in Figs. 8–10. Depending on the parameter ranges, the levels of discrepancy here are quite compatible with those previously characterized in [18, 20, 21] on former

versions of the IBM quantum processors, or even slightly better here for processors constantly evolving and improving. Despite these physical imperfections inherent to current experimental quantum processors available today, a good match is observed between theory and experiment in the results of Figs. 8–10, and this is obtained consistently over the whole range of the parameters  $(p, \gamma)$  tested for the qubit thermal noise. As a complement, a complete experimental state tomography, as in [20, 23, 24], could be envisaged for the output noisy qubit of the simulator circuit, and performed for every parameter configuration  $(p, \gamma)$ . This however would represent an infinite set of conditions which cannot be treated practically; and moreover whose detail and significance would be tied to a given quantum processor, while quantum processors are constantly being upgraded. For the present design, the tests of Figs. 8–10 consolidate the validation of the simulator circuit and its principle, as constructed here for the qubit thermal noise.

## 5. Conclusion

For the modeling of the qubit thermal noise, also known as generalized amplitude damping noise, we started from a standard quantum-operation model  $\mathcal{N}(\cdot)$  in Eq. (5) based on the four specific Kraus operators of Eqs. (1)–(4) and an associated qubit-environment model based on Eq. (14) from [8, 14]. The goal was then to exploit these modeling elements in order to construct a circuit model to simulate the qubit thermal noise  $\mathcal{N}(\cdot)$  on a quantum processor, with easy control on the noise parameters  $(p, \gamma)$ . From Eq. (14), we have deduced a proper Stinespring dilated model, as in Eq. (8), arranging for a control of the noise parameter  $p$  via an auxiliary qubit prepared in the state  $|p\rangle = \sqrt{p}|0\rangle + \sqrt{1-p}|1\rangle$  in Figs. 1 and 5. The Stinespring dilated representation has then been decomposed in terms of a few elementary operators, consisting of two-qubit Cnot operators and one-qubit rotation operators. The decomposition also arranges for an easy control of the other noise parameter,  $\gamma$ . The result of the decomposition has then been converted into a three-qubit simulator circuit expressed with the corresponding elementary quantum gates and shown in Fig. 5. The thermal noise simulator circuit obtained in Fig. 5 is an original circuit not previously reported to our knowledge, and offering a useful addition to existing libraries of quantum circuits. This simulator circuit has then been experimentally implemented, according to the layout of Fig. 6, on an IBM-Q quantum processor; and it has been experimentally tested and validated against the theoretical specifications of the thermal noise model. Through this worked-out example of a noise simulator circuit, this study also illustrates the generic methodology for exploiting such general-purpose quantum processors.

The present noise simulator circuit is constructed from the reference modeling approach of a non-unitary quantum map  $\rho \mapsto \mathcal{N}(\rho)$  based on the Kraus operators in Eqs. (1)–(5) and associated Stinespring dilation of Eq. (8). Accordingly, the model for the thermal noise  $\mathcal{N}(\cdot)$  exhibits the character of a functional-block type modeling, representing the action of the noise between an initial state when some processing

begins and a final state when it ends. Such a functional-block modeling is often relevant and employed in signals and systems theory. In this perspective, the present simulator circuit has application in many scenarios, in principle anywhere a controlled thermal noise need be simulated on a signal qubit. The simulator can serve to design and test the performance of optimal or efficient processings having to cope with thermal noise, according to the noise conditions. Quantum communication for instance offers such direction of application. Our simulator circuit provides a direct materialization of a quantum communication channel affected by thermal noise, and is well adapted to realize an input–output end-to-end simulation to investigate the noisy transmission across the channel, in a controlled way over the whole range of the channel parameters  $(p, \gamma)$ . Among interesting lines of investigation which can be addressed, optimal signaling configurations including the input signal states and their output measurements maximizing the input–output mutual information or achieving the information capacity, are not completely known, over the whole range of the channel parameters  $(p, \gamma)$ , especially when entangled signaling states of definite size are employed for communication, and in the parameter range where the channel is not entanglement-breaking and entangled inputs may improve over the independent-input capacity [8, 9, 25]. Other scenarios accessible to simulation could be the study of stochastic resonance effects, assigning a beneficial role to quantum noise or decoherence. Stochastic resonance phenomena represent the (counterintuitive) possibility of enhancing the performance of some processing when the amount of noise is increased up to an optimal nonzero level. For signal and information processing, stochastic resonance has been shown to occur in the classical domain under many forms [26–36], and in the quantum domain more recently [37–43]. In the quantum domain, the possibility of such stochastic resonance phenomena has been theoretically shown in [44–47] in operations of signal detection or estimation from noisy quantum signals affected by thermal noise. Experimental implementation, validation and exploration of such phenomena in controlled noise conditions are now accessible with the noise simulator of Figs. 5 and 6. Many other possibilities can be envisaged for applying quantum noise simulators, with controlled noise conditions, for investigations relevant to quantum signal and information processing.

This study also illustrates the possibilities made available for research on quantum technologies by the public access, through the internet cloud, to quantum processors, especially offering today an unparalleled platform for developments in quantum computation and quantum signal processing. Quantum processors, such as IBM-Q, are often exploited for quantum computation, to implement and test quantum algorithms under the form of unitary evolutions, expressed by means of elementary building blocks under the form of unitary quantum gates. This study relates to a slightly broader perspective, illustrating that non-unitary evolutions, such as quantum noise or decoherence, can as well be simulated on such quantum processors, under controlled conditions. Such possibilities are specially relevant to signal processing, which naturally has to cope

with noise while designing efficient processing, classical or quantum. The present circuit model for quantum thermal noise offers a tool to contribute in these directions.

## References

- [1] M. A. Nielsen and I. L. Chuang, *Quantum Computation and Quantum Information* (Cambridge University Press, Cambridge, 2000).
- [2] S. Haroche and J.-M. Raimond, *Exploring the Quantum: Atoms, Cavities, and Photons* (Oxford University Press, Oxford, 2006).
- [3] M. M. Wilde, *Quantum Information Theory* (Cambridge University Press, Cambridge, 2017).
- [4] W. P. Schleich *et al.*, Quantum technology: From research to application, *Appl. Phys. B* **122** (2016) 130.
- [5] J. Preskill, Quantum computing in the NISQ (noisy intermediate-scale quantum) era and beyond, *Quantum* **2** (2018) 79.
- [6] B. Ye and L. Qiu,  $1/f$  noise in Ising quantum computers, *Fluct. Noise Lett.* **13** (2014) 1450006.
- [7] F. Chapeau-Blondeau, Optimization of quantum states for signaling across an arbitrary qubit noise channel with minimum-error detection, *IEEE Trans. Inf. Theory* **61** (2015) 4500–4510.
- [8] S. Khatri, K. Sharma and M. M. Wilde, Information-theoretic aspects of the generalized amplitude-damping channel, *Phys. Rev. A* **102** (2020) 012401.
- [9] A. S. Holevo and V. Giovannetti, Quantum channels and their entropic characteristics, *Rep. Prog. Phys.* **75** (2012) 046001.
- [10] B. Vacchini, Quantum noise from reduced dynamics, *Fluct. Noise Lett.* **15** (2016) 1640003.
- [11] A. A. Abbott, J. Wechs, D. Horsman, M. Mhalla and C. Branciard, Communication through coherent control of quantum channels, *Quantum* **4** (2020) 333.
- [12] F. Chapeau-Blondeau, Quantum parameter estimation on coherently superposed noisy channels, *Phys. Rev. A* **104** (2021) 032214.
- [13] W. F. Stinespring, Positive functions on  $C^*$ -algebras, *Proc. Am. Math. Soc.* **6** (1955) 211–216.
- [14] M. Rosati, A. Mari and V. Giovannetti, Narrow bounds for the quantum capacity of thermal attenuators, *Nat. Commun.* **9** (2018) 4339.
- [15] A. Barenco, C. H. Bennett, R. Cleve, D. P. Di Vincenzo, N. Margolus, P. Shor, T. Sleator, J. A. Smolin and H. Weinfurter, Elementary gates for quantum computation, *Phys. Rev. A* **52** (1995) 3457–3467.
- [16] IBM Quantum Computing Platform, <https://quantum-computing.ibm.com> (Accessed 23 December 2021).
- [17] S. J. Devitt, Performing quantum computing experiments in the cloud, *Phys. Rev. A* **94** (2016) 032329.
- [18] N. M. Linke, D. Maslov, M. Roetteler, S. Debnath, C. Figgatt, K. A. Landsman, K. Wright and C. Monroe, Experimental comparison of two quantum computing architectures, *Proc. Natl. Acad. Sci. USA* **114** (2017) 3305–3310.
- [19] K. Choo, C. W. von Keyserlingk, N. Regnault and T. Neupert, Measurement of the entanglement spectrum of a symmetry-protected topological state using the IBM quantum computer, *Phys. Rev. Lett.* **121** (2018) 086808.

- [20] Y. Chen, M. Farahzad, S. Yoo and T.-C. Wei, Detector tomography on IBM quantum computers and mitigation of an imperfect measurement, *Phys. Rev. A* **100** (2019) 052315.
- [21] A. Shukla, M. Sisodia and A. Pathak, Complete characterization of the directly implementable quantum gates used in the IBM quantum processors, *Phys. Lett. A* **384** (2020) 126387.
- [22] S. Das, M. D. Rahman and M. Majumdar, Design of a quantum repeater using quantum circuits and benchmarking its performance on an IBM quantum computer, *Quantum Inf. Process.* **20** (2021) 245.
- [23] A. Gaikwad, K. Shende and K. Dorai, Experimental demonstration of optimized quantum process tomography on the IBM quantum experience, *Int. J. Quantum Inf.* **19** (2021) 2040004.
- [24] J. Zhang, K. Li, S. Cong and H. Wang, Efficient reconstruction of density matrices for high dimensional quantum state tomography, *Signal Process.* **139** (2017) 136–142.
- [25] H. Li-Zhen and F. Mao-Fa, The Holevo capacity of a generalized amplitude-damping channel, *Chin. Phys.* **16** (2007) 1843–1847.
- [26] K. Loerincz, Z. Gingl and L. B. Kiss, A stochastic resonator is able to greatly improve signal-to-noise ratio, *Phys. Lett. A* **224** (1996) 63–67.
- [27] V. Galdi, V. Pierro and I. M. Pinto, Evaluation of stochastic-resonance-based detectors of weak harmonic signals in additive white Gaussian noise, *Phys. Rev. E* **57** (1998) 6470–6479.
- [28] F. Chapeau-Blondeau, Noise-assisted propagation over a nonlinear line of threshold elements, *Electron. Lett.* **35** (1999) 1055–1056.
- [29] Z. Gingl, R. Vajtai and L. B. Kiss, Signal-to-noise ratio gain by stochastic resonance in a bistable system, *Chaos Solitons Fractals* **11** (2000) 1929–1932.
- [30] N. G. Stocks, Information transmission in parallel threshold arrays: Suprathreshold stochastic resonance, *Phys. Rev. E* **63** (2001) 041114.
- [31] L. B. Kish, G. P. Harmer and D. Abbott, Information transfer rate of neurons: Stochastic resonance of Shannon’s information channel capacity, *Fluct. Noise Lett.* **1** (2001) L13–L19.
- [32] F. Chapeau-Blondeau and D. Rousseau, Noise improvements in stochastic resonance: From signal amplification to optimal detection, *Fluct. Noise Lett.* **2** (2002) L221–L233.
- [33] M. D. McDonnell, D. Abbott and C. E. M. Pearce, A characterization of suprathreshold stochastic resonance in an array of comparators by correlation coefficient, *Fluct. Noise Lett.* **2** (2002) L205–L220.
- [34] M. D. McDonnell, N. G. Stocks, C. E. M. Pearce and D. Abbott, *Stochastic Resonance: From Suprathreshold Stochastic Resonance to Stochastic Signal Quantization* (Cambridge University Press, Cambridge, 2008).
- [35] A. Patel and B. Kosko, Optimal noise benefits in Neyman–Pearson and inequality-constrained statistical signal detection, *IEEE Trans. Signal Process.* **57** (2009) 1655–1669.
- [36] A. Delahaies, F. Chapeau-Blondeau, D. Rousseau and F. Franconi, Tuning the noise in magnetic resonance imaging to maximize nonlinear information transmission, *Fluct. Noise Lett.* **12** (2013) 1350005.
- [37] J. J. L. Ting, Stochastic resonance for quantum channels, *Phys. Rev. E* **59** (1999) 2801–2803.
- [38] G. Bowen and S. Mancini, Stochastic resonance effects in quantum channels, *Phys. Lett. A* **352** (2006) 272–275.
- [39] M. M. Wilde and B. Kosko, Quantum forbidden-interval theorems for stochastic resonance, *J. Phys. A* **42** (2009) 465309.

- [40] F. Caruso, S. F. Huelga and M. B. Plenio, Noise-enhanced classical and quantum capacities in communication networks, *Phys. Rev. Lett.* **105** (2010) 190501.
- [41] C. K. Lee, L. C. Kwek and J. Cao, Stochastic resonance of quantum discord, *Phys. Rev. A* **84** (2011) 062113.
- [42] C. Lupo, S. Mancini and M. M. Wilde, Stochastic resonance in Gaussian quantum channels, *J. Phys. A* **46** (2013) 045306.
- [43] N. Gillard, E. Belin and F. Chapeau-Blondeau, Stochastic resonance with unital quantum noise, *Fluct. Noise Lett.* **18** (2019) 1950015.
- [44] F. Chapeau-Blondeau, Qubit state estimation and enhancement by quantum thermal noise, *Electron. Lett.* **51** (2015) 1673–1675.
- [45] N. Gillard, E. Belin and F. Chapeau-Blondeau, Stochastic antiresonance in qubit phase estimation with quantum thermal noise, *Phys. Lett. A* **381** (2017) 2621–2628.
- [46] N. Gillard, E. Belin and F. Chapeau-Blondeau, Qubit state detection and enhancement by quantum thermal noise, *Electron. Lett.* **54** (2018) 38–39.
- [47] N. Gillard, E. Belin and F. Chapeau-Blondeau, Enhancing qubit information with quantum thermal noise, *Physica A* **507** (2018) 219–230.